doi:10.1016/j.jmb.2004.12.026 J. Mol. Biol. (2005) 346, 1109–1120

JMB

Available online at www.sciencedirect.com

SCIENCE DIRECT®

ELSEVIER

Lipid Rafts have Different Sizes Depending on Membrane Composition: A Time-resolved Fluorescence Resonance Energy Transfer Study

Rodrigo F. M. de Almeida[1,2]*, Luís M. S. Loura[1,3], Alexander Fedorov[1] and Manuel Prieto[1]

[1]*Centro de Química-Física Molecular, Instituto Superior Técnico, Universidade Técnica de Lisboa, Lisboa, Portugal*

[2]*Centro de Química e Bioquímica, Faculdade de Ciências de Lisboa, Ed. C8 Campo Grande, 1749-016 Lisboa Portugal*

[3]*Departamento de Química and Centro de Química Universidade de Évora, Rua Romão Ramalho, 59 P-7000-671 Évora, Portugal*

**Corresponding author*

The ternary lipid system palmitoylsphingomyelin (PSM)/palmitoyloleoylphosphatidylcholine (POPC)/cholesterol is a model for lipid rafts. Previously the phase diagram for that mixture was obtained, establishing the composition and boundaries for lipid rafts. In the present work, this system is further studied in order to characterize the size of the rafts. For this purpose, a time-resolved fluorescence resonance energy transfer (FRET) methodology, previously applied with success to a well-characterized phosphatidylcholine/cholesterol binary system, is used. It is concluded that: (1) the rafts on the low raft fraction of the raft region are small (below 20 nm), whereas on the other side the domains are larger; (2) on the large domain region, the domains reach larger sizes in the ternary system ($> \sim$75–100 nm) than in binary systems phosphatidylcholine/cholesterol (between $\sim$20 and $\sim$75–100 nm); (3) the raft marker ganglioside G_{M1} in small amounts (and excess cholera toxin subunit B) does not affect the general phase behaviour of the lipid system, but can increase the size of the rafts on the small to intermediate domain region. In summary, lipid–lipid interactions alone can originate lipid rafts on very different length scales. The conclusions presented here are consistent with the literature concerning both model systems and cell membrane studies.

Keywords: lipid rafts; sphingomyelin; cholesterol; FRET; ganglioside G_{M1}

Introduction

The model for lipid rafts was proposed based mainly on the fact that detergent-resistant membranes isolated from cellular membranes were enriched in (glyco)sphingolipids and cholesterol (chol), and depleted in (unsaturated) phosphatidylcholines (PCs), and also that the simultaneous presence of chol and sphingolipids was necessary to confer detergent insolubility to some proteins.[1]

On another hand, it was known that liposomes with resistance to solubilization with Triton X-100 (TX-100) are in ordered phases, namely, gel or solid ordered (so) and liquid ordered (lo), whereas in the liquid disordered (ld; phospholipid fluid phase) they are solubilized.[2] Given that the so phase is found in cell membranes only in exceptional cases and that detergent-resistant membranes isolated from cell membranes are rich in chol, it is currently accepted that rafts are the cellular equivalent of lo domains *in vitro*.[3]

Rafts and other microdomains in membranes of

Present address: Rodrigo F. M. de Almeida, Centro de Química-Física Molecular, Complexo I, IST, Av. Rovisco Pais, 1049-001 Lisboa, Portugal.

Abbreviations used: PSM, *N*-palmitoyl-D-sphingomyelin; POPC, 1-palmitoyl,2-oleoyl-*sn*-glycerophosphocholine; chol, cholesterol; lo, liquid ordered; TX-100, Triton X-100; ld, liquid disordered; so, solid ordered; *t*-PnA, *trans*-parinaric acid; DPH, diphenylhexatriene; T_m, main transition temperature; PC, phosphatidylcholine; DMPC, 1,2-dimyristoyl-*sn*-glycerophosphocholine; SM, sphingomyelin; CTB, cholera toxin subunit B; FRET, fluorescence resonance energy transfer; NBD-PE, *N*-(7-nitrobenz-2-oxa-1,3-diazol-4-yl)-dipalmitoylphosphatidylethanolamine; Rhod-PE, *N*-(lissamine™-rhodamine B)-dioleoylphosphatidylethanolamine; MLV, multilamellar vesicles; LUV, large unilamellar vesicles; $\langle r \rangle$, steady-state fluorescence anisotropy; E, FRET efficiency; X_{lo}, lo phase mole fraction; x_{chol}, chol mole fraction; DOPC, 1,2-dioleoyl-*sn*-glycero-3-phosphocholine.

E-mail address of the corresponding author: r.almeida@mail.ist.utl.pt

cells have usually been detected by indirect methods, such as detergent extraction, but this can increase the size of the pre-existing domains by at least one order of magnitude, as verified *in situ* by TX-100 treated fibroblast-like cells.[4] They can also be detected directly, but after, e.g. cross-linking of membrane components that leads to the formation of larger, otherwise undetectable, aggregates.[5,6] Some studies rely on the ganglioside G_{M1} as one of the most popular raft markers,[7] which is usually detected by addition of labelled cholera toxin subunit B (CTB).[8,9] CTB forms stable pentamers and, in this oligomeric state, is able to bind five G_{M1} molecules.[10] It is possible that this has an effect similar to cross-linking, thereby changing the size of the G_{M1} enriched domains.

Even with the use of sophisticated microscopic techniques, a clear consensus about the size, shape, and location of lipid rafts on cell membranes has not emerged.[11,12] Importantly, the work by Heerklotz and collaborators should be considered, as it shows that domains formed on the basis of PC/sphingomyelin (SM)/chol interactions are very sensitive to small perturbations: for the 1 : 1 : 1 mixture, an enthalpy of 2.5 kJ/mol includes both domain disintegration and ordered-to-disordered transition of the acyl chains.[13]

Recently, we determined the ternary phase diagrams *N*-palmitoyl-D-sphingomyelin (PSM)/1-palmitoyl-2-oleoyl-*sn*-glycerophosphocholine (POPC)/chol at room temperature (23 °C) and at 37 °C, and they were used to rationalize published data on these mixtures.[14] This is a system of the type low main-transition temperature (T_m) lipid/high T_m lipid/chol, which is thought to be the simplest system to model lipid rafts.[8,15] Two aspects should be highlighted: (i) the phase behavior of the mixtures was determined solely by methods that do not involve detergent extraction; (ii) some tie-lines that give the composition and fraction of the coexisting ld/lo phases were obtained, i.e. the composition and boundaries for lipid rafts were established. The ternary phase diagram at room temperature is reproduced in Figure 1, where some mixtures used in the present work are highlighted. The main features of the diagram are a broad lo/ld phase coexistence region on the left side of the diagram (high POPC/PSM ratio, persisting up to ~50 mol% chol), a considerable so/lo phase coexistence region and the presence of a tie-triangle, i.e. a region of three-phase coexistence. In the ld/lo coexistence region, the highlighted points are along the same tie-line, i.e. the composition of the coexisting phases is always the same, only the fraction of each phase changes. The extremes of the tie-line correspond to the rafts' composition (lo phase, closer to the top of the diagram) and the ld composition. This tie-line was chosen because it contains the PC/SM/chol 1 : 1 : 1 mixture, which is very popular for model raft studies.[16,17] Another advantage of using this tie-line is that due to thermodynamic restrictions it has a low uncertainty (a detailed discussion is found elesewhere[14] and below), making it very suitable for application of the fluorescence resonance energy transfer (FRET) methodology described below.

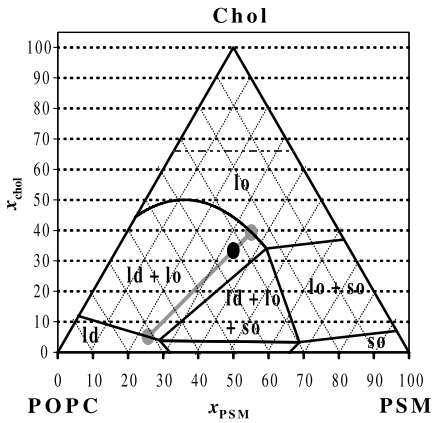

Figure 1. PSM/POPC/chol phase diagram at 23 °C.[14] The tie-line (grey line) is the one that contains the PSM/POPC/chol (1 : 1 : 1) mixture (black point) and is the one used in the present FRET study. The extremes of the tie-line (grey points) give the composition of the coexisting ld (low chol) and lo (high chol) phases. The broken line for a chol mol fraction of $x_{chol} = 0.66$ represents the solubility limit of chol in PC bilayers.

FRET has a strong dependence (sixth power) of its rate on the intermolecular distance, which has led to its wide use as a "spectroscopic ruler" for determination of distances in the 1–10 nm range.[18] If, instead of an isolated donor/acceptor pair at a single defined distance, there is a distribution of donor and acceptor molecules in a plane (as a lipid bilayer), donor fluorescence becomes dependent on the local acceptor concentration,[19] probing a larger length scale, but there are very few elegant studies with application of FRET to ternary systems of this type.[20,21]

Here, we apply a novel FRET methodology[22] to mixtures of PSM/POPC/chol. This methodology has been applied with success to binary phospholipid/chol mixtures,[23] and is now extended to the study of ternary mixtures. Labelled phospholipids were selected as fluorescent probes. *N*-(7-nitrobenz-2-oxa-1,3-diazol-4-yl)-dipalmitoylphosphatidylethanolamine (NBD-PE) was used as a FRET donor, and *N*-(lissamine™-rhodamine B)-dioleoylphosphatidylethanolamine (Rhod-PE) was the FRET acceptor.

It should be stressed that for ternary mixtures, as well as for binary systems, the determination of partition coefficients for probes should be made along a tie-line. To apply the FRET methodology developed in our laboratory, which gives information about the domains' size on the nanometer scale, the knowledge of the tie-lines (hence the phase diagram) is required. In fact, although indispensable, the phase diagram does not contain information about the size of the domains. As such, the present study completes the description of our lipid raft model.

This is the first time that FRET is systematically applied along a tie-line of a previously extensively characterized ternary lipid system containing chol. Furthermore, the effect of small amounts of the glycosphingolipid G_{M1}, which as already mentioned is one of the most popular raft markers in the presence or absence of CTB, on the size of the lipid rafts was also addressed.

Results

Firstly, the methodologies to determine phase boundaries were applied to the tie-line represented in the diagram of Figure 1. The determination of phase coexistence boundaries is described in detail elsewhere.[14] In the present work, because we were considering only ld/lo phase separation, we used the methods based on the steady-state anisotropy, $\langle r \rangle$, of diphenylhexatriene (DPH), and the lifetime weighted quantum yield of *trans*-parinaric acid (*t*-PnA). The lifetime-weighted quantum yield (because it is proportional to the fluorescence quantum yield; also designated by amplitude averaged lifetime) is defined by:[14,24]

$$\bar{\tau} = \sum_i \alpha_i \tau_i \qquad (1)$$

and the mean or average fluorescence lifetime is given by:

$$\langle \tau \rangle = \left(\sum_i \alpha_i \tau_i^2 \right) / \left(\sum_i \alpha_i \tau_i \right) \qquad (2)$$

for a decay described by a sum of exponentials, where α_i is the normalized pre-exponential and τ_i the lifetime of the decay component *i*.

Some of these measurements were performed both on multilamellar vesicles (MLV) and large unilamellar vesicles (LUV) to ensure that the phase behaviour was independent of the membrane model system used (results not shown). The measurements given in this study were carried out mainly to confirm the boundaries of the previously published diagram,[14] and to test if the addition of G_{M1} and CTB could affect the general phase behaviour of the system. The possible variations on the direction of the tie-line containing the 1 : 1 : 1 mixture and their influence on the results are discussed below. However, it can already be stated that the uncertainty interval is very narrow[14] and this approach, i.e. to carry out the study along a tie-line, is necessary in order to keep constant the composition of the coexisting phases. With other methods, e.g. for a fixed chol mol fraction, x_{chol}, or fixed proportion of non-chol components, not only the phase composition varies but also the type and number of phases present can change.[14]

In Figure 2(a), the anisotropy of DPH as a function of chol mole fraction is represented for different concentrations of G_{M1}. The trend of the results agrees with the phase boundaries, which

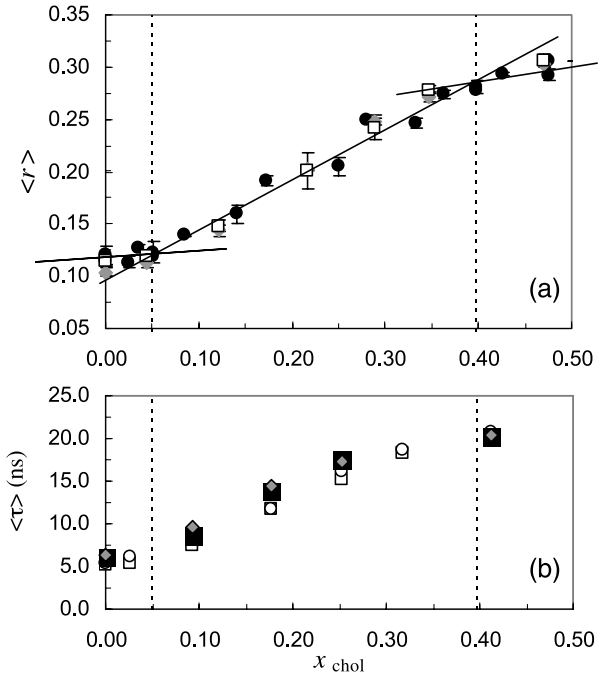

Figure 2. Determination of the ld/lo phase boundaries for the grey tie-line of Figure 1 from $\langle r \rangle_{DPH}$ in MLV (a) and detection of ordering effects from $\langle \tau \rangle_{t\text{-PnA}}$ in LUV (b) as a function of chol mole fraction (x_{chol}). The vertical dotted lines represent the phase boundaries taken from the phase diagram. In (a), the three data sets correspond to 0 mol% (●), 2 mol% (◆) and 4 mol% (□) G_{M1} (the latter two series also in the presence of excess CTB), and the three straight lines distinguish three regimes: only ld phase for low x_{chol}, ld/lo coexistence for intermediate x_{chol}, and only lo phase for high x_{chol}. In (b), the data sets correspond to no G_{M1}, no CTB (□), no G_{M1} and excess CTB (○), 2 mol% G_{M1} and no CTB (■), 2 mol% G_{M1} and excess CTB (◆).

linearity further supports the direction of the tie-line on the phase diagram, and it is not affected by the presence of up to 4 mol% G_{M1}. In Figure 2(b), the mean fluorescence lifetime of *t*-PnA is represented as a function of x_{chol}. This is one of the more sensitive parameters to the presence of ordered domains in membranes (although not useful to determine phase boundaries, contrary to the lifetime-weighted quantum yield[14]) because *t*-PnA, when in ordered phases, has an emission decay with a long component (>10 ns), which increases significantly the mean fluorescence lifetime of the probe. As can be seen in Figure 2(b), there is a very small increase in the order of the system when 2 mol% G_{M1} is present. The deviation between the samples with no G_{M1} (presence or absence of CTB) gives an estimation of the error associated to the measurements, because CTB, in principle, should have no effect on the liposomes without G_{M1}.

Secondly, the photophysical properties of both donor and acceptor probes were studied along the tie-line represented in Figure 1. In general, the trends displayed by the different parameters as a

function of lo phase mole fraction, X_{lo}, and the main features of the fluorescence decays (number, lifetime, and amplitude of the components; not shown) are identical to the previously characterized binary system 1,2-dimyristoyl-*sn*-glycero-3-phosphocholine (DMPC)/chol,[23] which further supports that data are being collected along a ld/lo tie-line.

The partition coefficient, K_p, of both NBD-PE and Rhod-PE were determined from the variation of the lifetime-weighted quantum-yield, $\bar{\tau}$, with X_{lo}, and that of Rhod-PE also from its steady-state fluorescence intensity, I_F (leading to the same value of K_p as the other method). Mole fractions are used both for probe concentration and phase fraction in the partition coefficient calculations (see Appendix).

The relevant expressions for partition coefficient calculation when no significant spectral shifts occur are:

$$I_F = K(\varepsilon_1\phi_1 K_p X_1 + \varepsilon_2\phi_2 X_2)/(K_p X_1 + X_2) \quad (3)$$

and

$$\bar{\tau} = (\bar{\tau}_1 K_p X_1 + \bar{\tau}_2 X_2)/(K_p X_1 + X_2) \quad (4)$$

where 1=lo, 2=ld phases, K is a normalization factor, ε_i is the molar absorption coefficient, ϕ_i the quantum yield, and $\bar{\tau}_i$ the lifetime-weighted quantum yield of the probe in phase i. $\varepsilon_1/\varepsilon_2$ is taken from the absorption spectra, and $\phi_1/\phi_2 = \bar{\tau}_1/\bar{\tau}_2$. From a fit of equation (3) to I_F *versus* X_{lo} data or equation (4) to $\bar{\tau}$ *versus* X_{lo} data, K_p is readily obtained.[23,24]

In the case of the donor probe (NBD-PE), the lifetime-weighted quantum yield varied between 8.4 ns and 9.6 ns (Figure 3(a)), and the mean fluorescence lifetime between 9.2 ns and 10.5 ns (results not shown). From the data in Figure 3(a), a value of $K_p = 4.3 \pm 1.2$ was obtained, showing a preference of this probe for the lo phase.

For the acceptor probe (Rhod-PE), both the lifetime and the steady-state fluorescence intensity show a strong decrease with X_{lo}, as reported for the DMPC/chol system,[23] and this was used to calculate the lo/ld partition coefficient for that probe (Figure 3(b)). The value recovered is $K_p = 0.37 \pm 0.06$. Thus, unlike the donor, Rhod-PE prefers the ld phase rather than the lo phase. The steady-state fluorescence anisotropy of Rhod-PE shows an interesting behaviour (Figure 3(c)). It decreases in the coexistence region, but it increases when the extreme of the tie-line corresponding to pure lo phase is reached. This is due to the presence of a very efficient energy homotransfer between Rhod-PE molecules[25] that leads to a strong emission depolarization. The anisotropy is lower in the lo phase than in the ld phase, because the lo phase has a much lower mean molecular surface area, and for the same analytical concentration, the surface density of Rhod-PE is higher in the lo phase. In this way, homotransfer is more efficient and a stronger depolarization occurs. The relative depolarization that occurs for a pure lo phase as compared to a pure ld phase is in very good agreement with the relative extent of depolarization

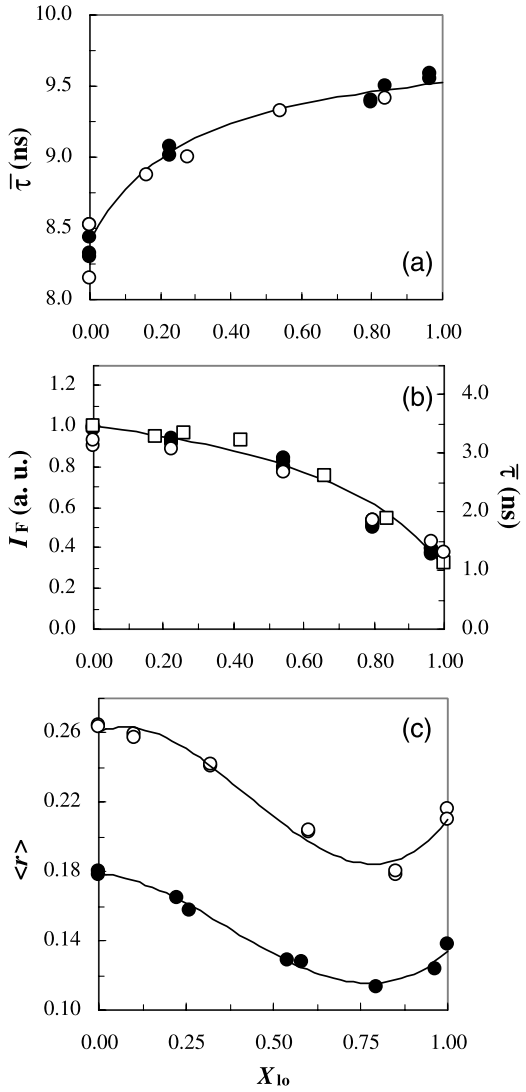

Figure 3. (a) Variation of $\bar{\tau}_{NBD-PE}$ in PSM/POPC/chol LUV, as a function of X_{lo}, along the grey tie-line of Figure 1, in the absence (●) and in the presence of 2 mol% G_{M1} (○). The line is the fitting curve using equation (4), with $K_p = 4.3 \pm 1.2$. (b) Variation of I_F (●) and lifetime-weighted quantum yield (○) of Rhod-PE in PSM/POPC/chol LUV, as a function of X_{lo}, along the grey tie-line of Figure 1. The line is the fitting curve using equation (3), with $K_p = 0.37 \pm 0.06$. Variation of I_F along the same tie-line for Rhod-PE in the presence of 2 mol% G_{M1} and excess CTB (□). (c) Variation of $\langle r \rangle_{Rhod-PE}$ in PSM/POPC/chol LUV with compositions containing the grey tie-line of Figure 1, as a function of X_{lo}, for two Rhod-PE/total lipid mole ratios: 1 : 200 (●) and 1 : 500 (○). The lines are merely guides to the eye.

predicted by the model described by Snyder & Freire[26], calculated for a critical distance for FRET between Rhodamine fluorophores in fluid lipid bilayers of $R_0 = 64.1$ Å,[25] showing that the probe distribution is the same in both pure phases (of course, in the coexistence range, the probe distribution is ruled by the partition coefficient). The trend of the steady-state anisotropy is shown for

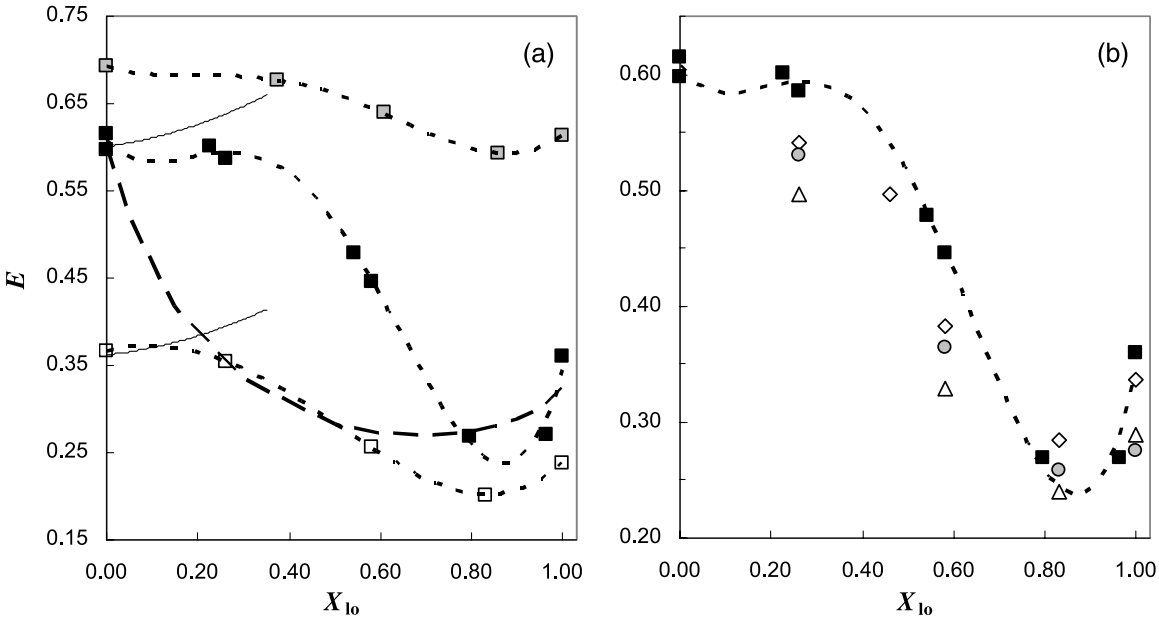

Figure 4. Variation of E between the donor/acceptor pair NBD-PE/Rhod-PE in PSM/POPC/chol LUV, as a function of X_{lo}, along the grey tie-line of Figure 1. (a) Effect of acceptor concentration and comparison with the binary system DMPC/chol. The dotted lines are merely guides to the eye. The thin continuous lines are the values of E calculated for a random distribution of donor and acceptor molecules in hypothetical pure ld phase (see Appendix) for acceptor/lipid ratios of 1 : 200 and 1 : 500. The different data sets correspond to 1 : 200 acceptor lipid ratio (■); 1 : 500 acceptor lipid ratio (□), and, for comparison, the values for the binary system DMPC/chol along the ld/lo tie-line at 30 °C are also shown (▩).[23] The theoretical line for infinite phase separation (large domains; see Appendix) for the 1 : 200 acceptor/total lipid mole ratio is also shown (thick broken line). (b) Effect of raft markers. The different data sets correspond to 1 : 200 acceptor lipid ratio, with 0 mol% G_{M1} and 2 mol% G_{M1}/no CTB indistinguishable (■), 2 mol % G_{M1} and excess CTB (◇), 4 mol% G_{M1} and no CTB (●), 4 mol% G_{M1} and excess CTB (△).

two acceptor concentrations (1 : 200 and 1 : 500 relative to total lipid). The relative extent of depolarization when going from the lower to the higher probe concentration in each pure phase is also in agreement with the predictions of the theoretical model,[26] which assumes a random distribution of probe in the bilayer, thus showing that the acceptor is randomly distributed in each pure phase at both concentrations studied, which is also an assumption of the FRET models used here (see Appendix). In the coexistence region, the existence of two separated phases leads to a further local enrichment of probe, an effect that only disappears when a one-phase situation is reached again. This justifies the minimum in the curves of Figure 3(c).

Finally, the efficiency of FRET along the tie-line, its variation with acceptor concentration and different amounts of G_{M1} and absence/presence of CTB were obtained (Figure 4). The experimental values of E for the binary mixture DMPC/chol[23] with an acceptor/total lipid mole ratio of 1 : 200 are also shown. The general trend of the results is similar in all cases, and is shown to be independent of the total acceptor concentration.

In order to obtain the experimental curves, a series of samples with compositions spanning a tie-line with donor only (D series) was prepared, and another series of samples prepared with the same lipid composition, but with both donor and acceptor (DA series). The FRET efficiency, E, is calculated for each pair of samples through the relationship:

$$E = 1 - \left(\int_0^\infty i_{DA}(t)\mathrm{d}t\right) / \int_0^\infty i_D(t)\mathrm{d}t$$
$$= 1 - \bar{\tau}_{DA}/\bar{\tau}_D \qquad (5)$$

In this way, a curve of E *versus* X_{lo} is obtained. One advantage of representing E *versus* X_{lo} is that the results for different systems displaying ld/lo phase separation can be compared more directly (the abscissa scale is the same).

In the absence of raft markers, two acceptor/total lipid mole ratios were used (1 : 500 and 1 : 200) and both display the same trend (Figure 4(a)). This shows that the system is not perturbed by the presence of the acceptor probe, even at the highest concentration employed (0.5 mol%). Because the effect (absolute variation of E) is much larger for the 1 : 200 ratio (in fact, this variation is around the value of $E = 0.50$, and thus corresponds to the range in which this parameter is more accurately determined and sensitive to donor–acceptor separation[27]), and the published results for the binary system DMPC/chol concern also an acceptor/total lipid mole ratio of 1 : 200, the discussion will be more focused on this data subset.

From the results in Figure 4(a), it is clear that E

decreases inside the phase coexistence range, and increases again at the phase coexistence limit. This happens because donor and acceptor have different partitioning preferences, as shown above. When phase separation occurs, the acceptor concentration around the majority of donors is reduced, leading to less donor quenching and smaller E. For higher chol and PSM concentration, there is a single phase again, and this compartmentalization effect disappears. The presence of 2 mol% G_{M1} (Figure 4(b)) has no effect on E (the values are virtually indistinguishable of those obtained for 0% G_{M1}). Yet, the presence of 2 mol% G_{M1} and excess of CTB has a significant effect, similar to the one of 4 mol% G_{M1} in the absence of CTB. The addition of CTB to samples with 4 mol% G_{M1} further increases this effect. Interestingly, at the end of the curve, i.e. when lo is the dominant phase, G_{M1} and CTB have no influence on the trend of E. They only change in E value significantly up to approximately two-thirds of lo (molar fraction), where the values of E are lower then for the samples with no G_{M1}. As already shown, the phase behaviour is not affected by the presence of the ganglioside. Further support for this are the facts that the lifetime of the donor (in the absence of acceptor) and the partition coefficients of the probes also remain unchanged in the presence of G_{M1} and CTB (Figure 3(a) and (b)). The time-resolved FRET measurements are extremely reproducible (variations of less than 1.5% between independent samples prepared and ran in different days), thus all variations discussed are significant. The only parameter affected by higher amounts of G_{M1} is E. Consequently the changes observed on E must be due to topological effects (changes in, e.g. donor quantum yield or acceptor absorption spectrum are ruled out).

To obtain more information about the size of the domains, theoretical predictions of the FRET efficiency were made. The values of E calculated for a random distribution of probes in the ld phase (based on the photophysical parameters of the probes and the dimensions of the lipid bilayer; see Appendix) for the ternary system and the two acceptor concentrations used are also shown. Furthermore, for the 1 : 200 acceptor/total lipid mole ratio, the theoretical curve for infinite phase separation (i.e. very large domains; see Appendix) was calculated and is also shown in Figure 4(a).

Discussion

The tie-line that contains the PSM/POPC/chol equimolar mixture, determined by us,[14] was further supported in here by additional experimental evidence. Firstly, we show that the uncertainty associated with the tie-line is very small on the basis of the published phase diagram thoroughly co-substantiated by theoretical considerations and a large amount of experimental determinations.[14] The tie-line is severely restricted, due to: (i) limitations to the x_{chol} of the phase boundaries: for the studied PC and SM in the literature, the lo phase appears for low x_{chol},[28] usually between ~5 mol% and ~10 mol%. The attainment of a single lo phase occurs between the value of x_{chol} for POPC/chol (44 mol%) and PSM/chol mixtures (37 mol%) (this would not occur only for lower PSM fractions[14,29]), which implies that *a priori* the heights of the extremes of the tie-line have to lie within these narrow intervals, and that the experimental determinations that led to the construction of the phase diagram narrowed down even more these intervals. (ii) Restrictions on the tie-line slope: due to the configuration of the diagram, for the ld/lo coexistence region any tie-line has a direction between a parallel to the left side of the diagram (slope = 2; maximum) and a parallel to the left side of the tie-triangle (slope = 1.0; minimum). Furthermore, all evidence in the literature points to the enrichment in SM content when going from the ld to the lo phase; this means that the slope of the tie-line has to be <2, but because POPC alone forms lo phase, the enrichment in PSM is not as accentuated as for a mixture with a PC unable to form lo phase, as 1,2-dioleoyl-*sn*-glycero-3-phosphocholine (DOPC).[14,28] In fact the slope of the tie-line in Figure 1 is 1.2. On the other hand, since no tie-lines may ever cross, and the sides of the tie-triangle are also tie-lines, the slope has to be <1.3. Since the variation of the tie-lines direction is "fan-like", and the tie-line under consideration is close to the tie-triangle, it is expected that the slope is close to the maximum possible value.

Secondly, there is additional experimental evidence that the compositions used in this study essentially span a tie-line: linearity of $\langle r \rangle$ of DPH and lifetime-weighted quantum yield of *t*-PnA with slope changes occurring at the expected x_{chol}; good fits of relationships considering a partition coefficient between two phases for donor and acceptor probes. From the phase diagram and the additional experimental evidence a maximum uncertainty of 2% in x_{chol} for the extremes of the tie-line is reached. All the previous arguments allow carrying out a characterization of the domains size based on the variation of the efficiency of time-resolved FRET along the tie-line represented in Figure 1.

NBD-PE, the donor probe used in this work, is used in microscopy studies as a probe for the lo phase,[8] and here it is shown that it has a preference for that phase. The lo/ld K_p value obtained here is larger than the one determined for the binary system DMPC/chol, in agreement with a recent study of lo/ld and raft/non-raft NBD-labelled lipid partitioning.[30] Rhod-PE, on another hand, prefers the ld phase, as usually reported.[31]

The general variation of E along the tie-line (Figure 4) was explained in Results. However, important comparisons remain to be done. In fact, the value of E calculated for a random distribution of probes (continuous lines; Figure 4(a)) coincides with the experimental value measured for the extreme of the tie-line, corresponding to 100% ld for both acceptor/lipid ratios used (1 : 200 and

1 : 500). This validates the interpretation of the variations. The other feature that should be highlighted is that E only starts to decrease for X_{lo} higher than approximately 35%. This means that for $X_{lo} <$ 35%, the lo domains are so small that the donor continues to sense a near uniform distribution of acceptor in its vicinity. This effect is similar to that observed for binary DMPC/chol systems.[23] If a single ld phase is considered to persist up to ~35 mol% lo (corresponding to almost 20 mol% chol), i.e. where no decrease of E value is experimentally observed, the corresponding calculated efficiency would increase with X_{lo} due to the mean surface area reduction that is taking place (POPC is being replaced by PSM and chol; see Appendix). This shows that, contrary to the intuitive interpretation, invariance of E value in this system is indicative of domain formation (phase separation). However, the domains are too small to overcome the effect of mean molecular surface area reduction, and E does not decrease. Additionally, if the compositions for which there is no variation of E were not considered as part of ld/lo phase separation, then for calculation of K_p of the probes, only the points for higher X_{lo} would be considered. For both donor and acceptor, the shape of the curve (Figure 3(a) and (b)) would be completely changed, and in fact, the trend of the data would be closer to linearity, i.e. the recovered K_p would be closer to unit. In this way, the maximum decrease observed in E (that would be obtained for an infinite phase separation situation; see below) would not be as large as that observed experimentally (Figure 4). In summary, no matter how small the lo domains may be in the beginning of the tie-line of Figure 1, they still have to be considered as part of the ld/lo phase coexistence region, and for determination of the composition of the coexisting phases (extremes of the tie-line) they have to be taken into account.

For higher X_{lo}, the domains become larger, and the value of E shows a strong decrease, going through a minimum.

Again, this has been verified for the system DMPC/chol (Figure 4(a)). This is probably the reason why the presence of G_{M1} and CTB only affect E on the low X_{lo} side of the tie-line (Figure 4(b)). Their effect is to reduce E, which means increasing the size of the domains (rafts). If on the other side of the tie-line the domains are already large, the effect of G_{M1} and CTB, if any, is unnoticeable.

In Figure 5, along with the phase diagram of Figure 1, schematic illustrations of the domain structures are represented, with the best estimates for raft sizes in different regions of the diagram. It is not possible to estimate precisely the size of the domains; however, upper and lower bounds can be given. An upper limit for the lo phase domains (rafts) when these represent less than 35 mol% can be obtained through comparison with numerical simulations where domain sizes can be explored, and the probes (donor and acceptor) are distributed according to their partition coefficients.[23] The

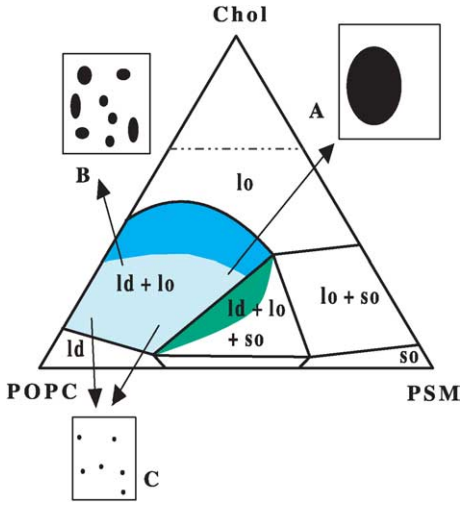

Figure 5. PSM/POPC/chol phase diagram at 23 °C, showing also the boundaries and schematic illustrations of the size of lipid rafts. Rafts are present in the blue-shaded area (ld/lo, coexistence). In the darker area, lo predominates over ld, and the reverse occurs for the light-shaded area. Rafts can also exist in the green-shaded area, where there is coexistence of three phases, but the so phase is present only in very low amounts. Insets: (a) region of large rafts; detected by microscopy and FRET (>75–100 nm); (b) region of intermediate size rafts: detected by FRET but not by microscopy (between ~20 nm and ~75–100 nm); (c) region of small rafts: not detected by FRET or microscopy (<20 nm).

fluorescence decay of the donor is then obtained from the molecule distribution. The decay is then analysed as if it were an experimental decay, and an apparent partition coefficient of the acceptor is recovered. If the domains are very large, the recovered value should be close to the value that generated the molecule distribution. In case that the domains are small, and energy transfer between probes in contiguous domains is probable, the recovered (apparent) partition coefficient is closer to unit, because FRET is closer to the expected on the basis of a random distribution. These simulations were also carried out[23] for lo/ld coexistence with a NBD-Rhodamine donor–acceptor pair, a $R_0 \sim 50$ Å, a K_p (donor) = 1.0, and K_p (acceptor) = 0.5, where R_0 is the critical Förster distance for FRET (see Appendix). In those simulations, for domain size $\sim 4R_0$, the recovered partition coefficient for the acceptor probe is closer to unit than the input value, but sufficiently distinct to allow for phase separation detection by FRET. This implies that the domains that result in a FRET efficiency identical to random distribution have to be certainly $< 4R_0$. In the present case, with a calculated value of $R_0 =$ 50 Å (equation (A1)), the lo domains (rafts) on the low X_{lo} side of the tie-line are, therefore, certainly below 20 nm.

Phase separation was observed by atomic force microscopy (AFM) for mixtures of brain SM/DOPC/chol,[32] where the presence of 10 mol%

chol practically does not affect the monolayer topology, whereas it is strongly affected by 20 mol% chol. For the mixture 1 : 1 : 1 a predominance of the ordered domains is observed. All these observations are in very good agreement with ours, because for 10 mol% chol, X_{lo} is very low and the size of the domains is very small, whereas for 20% chol, X_{lo} should be approximately 40% (Figure 1) where the domains are larger. For the 1 : 1 : 1 composition, the phase diagram predicts 80% for X_{lo}, but the domains of the ld phase, although few, are large (small E value), and thus observable, consistent with the predominance of the ordered domains reported.[32] This is certainly related to the choice of the proportion (2 : 1 : 1) PC/SM/chol for the raft mixture in the POPC containing system in a microscopy study[8] (instead of 1 : 1 : 1 as for DOPC), in order to have lo domains in a ld matrix, instead of the opposite (dark blue *versus* light blue; Figure 5).

Although the general trend of the results has many analogies to that observed for the binary system PC/chol, there is one very important difference. In the binary system, the decrease in E value was at most 20%, whereas in the ternary system PSM/POPC/chol modelling lipid rafts, it surpasses 50% (Figure 4). This means that phase separation is more pronounced in the ternary, rather than in the binary system. The domains in the binary system, even in the large domain side of the tie-line probably do not reach the size of the domains in the ternary system (Figure 5). The maximal effect on FRET ("infinite phase limit"[19]) occurs when boundary effects disappear, i.e. when the domains are large enough so that the number of probes near the interfaces between domains is small compared to those in the bulk of the domain, which for a circular domain corresponds to 15–20R_0 (~75–100 nm). Note that in the numerical simulation performed for domains of size 9R_0, the recovered K_p values were still closer to unit than the input values, showing that FRET near the interfaces is detectable.[23] The E *versus* X_{lo} curve predicted for very large domains (infinite phase separation; see Appendix) and acceptor/total lipid at a 1 : 200 mole ratio (thick broken line; Figure 4(a)) crosses the trend line of the experimental data at $X_{lo} \sim 0.75$. This corresponds to a situation where rafts occupy ~50% of the membrane surface area, in agreement with recent sophisticated studies in cell membranes (see below).

In our previous work[14] we posed the following question: why is it that in fluorescence microscopy with ~33 mol% chol two phases are seen and not in e.g. the binary mixtures POPC/chol (2 : 1)[8] or DPPC/chol (2 : 1) by AFM[33]? We proposed that in the ternary system, the compositional difference between ld and lo phases is higher (there is one more degree of freedom), and the properties of the coexisting phases may be more distinct, allowing for larger domains (in the optical microscopy experiment cited, 1 pixel corresponds to 80 nm). This hypothesis raised by us is consistent with the FRET results here presented. In fact, to date, in all cases reported in the literature, giant unilamellar vesicles that exhibit micron-scale liquid–liquid phase separation contain a minimum of three components: a high T_m lipid, a low T_m lipid and chol.[15] Although ld/lo phase separation in PC/chol binary mixtures is well-documented,[14] this is not observed by microscopy.

Another important conclusion from the present study is that the presence of small amounts of G_{M1} (raft marker), especially when associated with CTB, affect the topology of the domains, although the general macroscopic phase behaviour is not altered (Figure 4(b)). Nevertheless, because 2 mol% G_{M1} has no influence on E value and the presence of CTB or higher amounts of ganglioside, only affects the domains' size when these are relatively small, the domains detected with those raft markers in GUV by microscopy are probably not induced by the presence of the markers, because the domains observed by such techniques are larger and the amounts of G_{M1} used are usually smaller. For instance, the effect of 1 mol% G_{M1} on the topology of the raft-like domains in GUV prepared from extracts of brush border membranes was described.[9] The shape of the domains is somehow different when the ganglioside is present, but the size of the domains is of the same order of magnitude. It was reported that chemical cross-linking of raft components (glycosylphosphatidylinositol-anchored proteins) in living cells led to a clustering much less extensive than when the cells were treated with a non-ionic detergent, even in a concentration well below the usual concentration used in detergent extraction experiments.[34]

Unclustered rafts in cell membranes appear to have diameters below 100 nm,[7,35] below the resolution of optical microscopy. This corresponds to the size of rafts detected in the present FRET study. In fact, the results presented here correlate very well with some studies in cell membranes. Recently, immunogold electron microscopy *in situ* detection of rafts at high resolution pointed to an average diameter of 44 nm, and occupying 35% of the cell surface.[36] This corresponds to a fraction of ~50 mol% rafts (rafts are supposedly more densely packed than the rest of the membrane, and in this calculation we considered the raft/non-raft surface area ratio being equal to the lo/ld surface area ratio), for which our study indicates a size between ~20 nm and ~75–100 nm. In the Introduction, it was referred that TX-100 can increase the size of *in situ* visualized rafts by at least one order of magnitude.[4] On another hand, it is known that TX-100 stabilizes and even promotes the formation of lo domains in model membranes.[37] Here, it is shown that the size of the lo domains (rafts) increases considerably when the fraction of lo domains increases, establishing a link between the two previously cited studies. One important question now arises: what is the best model for lipid rafts, the small domains detected by spectroscopic techniques or the micron-sized domains observed in GUV by fluorescence microscopy? Micron (μm)

sized domains are important for visualization, dynamic (e.g. fluorescence correlation spectroscopy, single particle tracking) studies, and probably resemble aggregated raft in cells, whereas nanoscopic domains, as detected by FRET or fluorescence quenching,[38] resemble non-aggregated rafts. The physical origin of the small size of unclustered lipid rafts was reviewed recently.[12] Although several studies indicate that lipid-dependent clusters in cell membranes can be quite small,[7,35,39] it is known that there is a gradient in chol and SM concentrations from the endoplasmic reticulum, through the Golgi complex, to the plasma membrane,[40] and that the formation of large platforms is important for cellular functions as signalling or sorting.[6]

Here, it is shown that the size of lipid rafts depends on the membrane composition in (at least) three ways: (i) the complexity of the system (e.g. binary *versus* ternary; absence or presence of ganglioside); (ii) very importantly, the fraction of lo phase; and (iii) the presence of multivalent lipid-binding proteins. The first two involve only lipid–lipid interactions, and suffice to generate rafts with very different sizes.

Materials and Methods

Chemicals

POPC, NBD-PE, and Rhod-PE were purchased from Avanti Polar Lipids (Birmingham, AL). PSM (semi synthetic from bovine brain SM), chol, G_{M1} from bovine brain, and CTB from *Vibrio cholerae* were purchased from Sigma (St. Louis, MO). DPH and *t*-PnA were obtained from Molecular Probes (Eugene, OR).

Liposome preparation

MLV containing the appropriate lipids and DPH, NBD-PE, and Rhod-PE when used were prepared by standard procedures.[41] In the present case, because lipid mixtures are always used, above the T_m value should be interpreted as referred to the highest T_m value of the pure lipids present in the mixture. The suspension medium was 10 mM sodium phosphate, 150 mM NaCl, 0.1 mM EDTA (pH 7.4) (as in the determination of the ternary phase diagram[14]) or 0.05 M Tris, 200 mM NaCl 200, 3 mM NaN_3, 1 mM EDTA 1 (pH 7.5) (because the CTB used contains this salts). The results obtained were independent of the buffer (not shown). *t*-PnA was added from ethanol stock solution to the MLV suspension and the samples were re-equilibrated by freeze–thaw cycles and incubation above the T_m value.[42] All the FRET measurements were performed in LUV to avoid a multilayer geometry.[43] LUVs were obtained from MLV by the extrusion technique.[41] LUVs were also used in all measurements with CTB, because otherwise the protein could not interact with the inner bilayers of the MLV. CTB was added from a concentrated stock solution (buffer) to the samples, which were then incubated for several hours. In this way, lipid composition, and donor and acceptor surface density (the relevant parameter for FRET) were exactly the same for samples with and without CTB, and thus even small effects on the experimentally determined value of E can be appreciated and are significant.

The probe/lipid ratios used were 1 : 200 for DPH and Rhod-PE, 1 : 500 for *t*-PnA and Rhod-PE and 1 : 1000 for NBD-PE. For steady-state fluorescence anisotropy, $\langle r \rangle$, of DPH and fluorescence intensity decays, $i(t)$, of *t*-PnA measurements, the total lipid concentration was 0.1 mM. For FRET measurements, the total lipid concentration was 0.5 mM. The resulting probe/lipid ratios and total probe concentrations and absorbances are similar to those used by others.[44,45] The highest absorbance was verified for Rhod-PE 1 : 200, in 0.5 mM total lipid samples for which $A_{max} \sim 0.12$. Even in this case, a normalized curve for steady-state intensity and lifetime-weighted quantum yield are overlapped (Figure 3(b)); no artefacts such as inner filter effect, are, thus affecting the results. Nevertheless, the FRET efficiency is always measured from donor fluorescence (maximum absorbance at 428 nm ~ 0.003).

As a consequence of the preparation procedure, the probes are symmetrically distributed between the two bilayer leaflets.

The PSM and POPC concentration in stock solutions were confirmed by phosphorus analysis.[46] Probe concentrations were determined spectrophotometrically: ε(*t*-PnA, 299.4 nm, ethanol) $= 89 \times 10^3\ M^{-1}cm^{-1}$,[47] ε(DPH, 355 nm, chloroform) $= 80.6 \times 10^3\ M^{-1}cm^{-1}$,[48] ε(NBD-PE, $\lambda_{max} = 458$ nm, chloroform) $= 21 \times 10^3\ M^{-1}cm^{-1}$, and ε(Rhod-PE, $\lambda_{max} = 559$, chloroform) $= 95 \times 10^3\ M^{-1}cm^{-1}$.[49]

To guarantee equilibration of the lipid mixtures, they were kept at least overnight before the measurements began. Some measurements were repeated for longer incubation times yielding essentially the same results (not shown).

Absorption and fluorescence measurements

The absorption and steady-state instrumentation was the same as described.[24] All measurements were performed at room temperature (23 °C).

Absorption spectrophotometry measurements were performed as described.[24] Steady-state anisotropy measurements with DPH were performed as described.[14] For all other measurements, 0.5 cm × 0.5 cm cuvettes were used. For time-resolved measurements with *t*-PnA, the excitation wavelength was 303 nm (secondary laser of Rhodamine 6G[22]), and the emission was collected at 405 nm.

NBD-PE was excited at 428 nm (in the time-resolved case, a Ti:Sapphire laser was used). This wavelength was chosen instead of the absorption peak ($\sim$465 nm) to avoid absorption by Rhod-PE. The experimental layout consists of a diode-pumped solid state Nd:YVO_4 laser (Spectra Physics Milennia Xs, Darmstadt, Germany) that pumps the Tsunami mode-locked Ti:Sapphire laser (Spectra Physics). The output pulses of the Tsunami laser (pulse duration $<$100 fs, repetition rate $\sim$80 MHz, tuning range 700–1000 nm) were selected by the Pulse Picker (APE, Haus, Germany) to reduce the repetition rate to 4 MHz and afterwards are frequency doubled in a 1.5 mm LBO crystal with efficiency $\sim$40%. The emission was collected at 536 nm. For Rhod-PE, excitation and emission wavelengths were 570 nm and 593 nm, respectively (steady-state fluorescence) and 575 nm and 610 nm, respectively (time-resolved fluorescence; excitation with a secondary laser of Rhodamine 6G).

Acknowledgements

This work and research grants (BPD/17842/2004 to R.F.M. de A., and BPD/11488/2002 to A.F.) were supported by POCTI/FCT, Portugal.

Appendix

The critical distance for energy transfer, R_0, was calculated from:

$$R_0 = 0.2108\left[\kappa^2\Phi_D n^{-4}\int_0^\infty I(\lambda)\varepsilon(\lambda)\lambda^4 d\lambda\right]^{1/6} \quad (A1)$$

where κ^2 is the orientation factor, Φ_D is the donor quantum yield in the absence of acceptor, n is the refractive index, $I(\lambda)$ is the normalized donor emission spectrum, and $\varepsilon(\lambda)$ is the acceptor molar absorption spectrum (expressed in units of M^{-1} cm^{-1}). If the λ units used in equation (A1) are nm, then the calculated R_0 value has Å units. Values of $\kappa^2=2/3$, and $n=1.4$ were considered.[24] The fluorescence quantum yield $\Phi_D=0.33$ was estimated on the basis of the donor's lifetime-weighted quantum yield.[23]

Because R_0 is not small with respect to the membrane thickness, both in-plane transfer and out-of-plane transfer (to acceptors in the other membrane leaflet) were considered.[19]

For the in-plane FRET, the decay of donor fluorescence in the presence of acceptor, assuming a radius of exclusion of acceptors (R_e) around the donor (in this case the sum of the van der Waals radii of the chromophores), and a random distribution in the plane of the membrane considered as infinite, becomes:

$$\rho_{cis}(t) = \exp\left\{-\pi R_0^2 n\gamma\left[\frac{2}{3},\left(\frac{R_0}{R_e}\right)^6(t/\bar{\tau})\right](t/\bar{\tau})^{1/3} + \pi R_e^2 n\left(1-\exp\left[-\left(\frac{R_0}{R_e}\right)^6(t/\bar{\tau})\right]\right)\right\} \quad (A2)$$

where n is the surface density of acceptors and:

$$\gamma(x,y) = \int_0^y z^{x-1}\exp(-z)\,dz \quad (A3)$$

is the incomplete Gamma function.

The donor decay resulting from the transfer to acceptors in the apposing membrane leaflet is given by:

$$\rho_{trans}(t) = \exp\left\{-\frac{2c}{\Gamma(2/3)b}\int_0^{w/\sqrt{w^2+R_e}}[1-\exp(-tb^3\alpha^6)]\alpha^{-3}d\alpha\right\} \quad (A4)$$

where:

$$c = \Gamma(2/3)n\pi R_0^2\bar{\tau}^{-1/3} \quad (A5)$$

In this equation, Γ is the complete gamma function, $b=(R_0/w)/\bar{\tau}^{1/3}$, and w is the interplanar donor–acceptor distance. This value was fixed as $w=40$ Å for ld phase and $w=49$ Å for lo phase.[50]

The donor decay in the presence of acceptor becomes:

$$i_{DA}(t) = i_D(t)\rho_{cis}(t)\rho_{trans}(t) \quad (A6)$$

and the FRET efficiency (E) is computed numerically using equation (5).

In the calculation of the surface density of acceptors, an area per molecule of 66.4 $Å^2$ for POPC.[51] 47.8 $Å^2$ for PSM[52] and 37.7 $Å^2$ for Chol[53] were considered. The condensation effect of chol was taken into account.[53]

If phase separation occurs, it is possible to calculate the value expected for E in the case that the domains are very large (infinite phase separation limit).[19,23,24] The donor decay in the absence of acceptor is given by:

$$i_D(t) = x_1 i_{D1}(t) + x_2 i_{D2}(t) \quad (A7)$$

where x_i is the mole fraction and $i_{Di}(t)$ the fluorescence decay of the donor in phase $i=1$, 2. The donor decay in the presence of acceptor is given by:

$$i_{DA}(t) = x_1 i_{D1}(t)\rho_{cis1}(t)\rho_{trans1}(t) + x_2 i_{D2}(t)\rho_{cis2}(t)\rho_{trans2}(t) \quad (A8)$$

where $\rho_{cis,\,i}(t)$ and $\rho_{trans,\,i}(t)$ are calculated as for the one phase situation (equations (A2)–(A5), respectively), but the parameters adequate to each phase have to be considered. These are the ones that originate a value of E correspondent to the extremes of the experimental curve. The partition coefficient is defined by:

$$K_p^{1/2} = \frac{n_1/X_1}{n_2/X_2} \quad (A9)$$

where X_i is phase i mole fraction. In this way, for a chosen value of $X_1=X_{lo}=1-X_{ld}$, the fraction of probe in each phase can be calculated. Following equations (A7) and (A8), the FRET efficiency is calculated numerically through equation (5), and a theoretical curve of E *versus* X_{lo} for large domains is then obtained, which can be compared with the experimental results.

References

1. Simons, K. & Ikonen, I. (1997). Functional rafts in cell membranes. *Nature*, **387**, 569–572.
2. Schroeder, R., London, E. & Brown, D. (1994). Interactions between saturated acyl chains confer detergent resistance on lipids and glycosylphosphatidylinositol (GPI)-anchored proteins: GPI-anchored proteins in liposomes and cells show similar behavior. *Proc. Natl Acad. Sci. USA*, **91**, 12130–12134.
3. London, E. & Brown, D. A. (2000). Insolubility of lipids in Triton X-100: physical origin and relationship to sphingolipid/cholesterol membrane domains (rafts). *Biochim. Biophys. Acta*, **1508**, 182–195.
4. Giocondi, M.-C., Vié, V., Lesniewska, E., Goudonnet,

J.-P. & Le Grimellec, C. (2000). *In situ* imaging of detergent-resistant membranes by atomic force microscopy. *J. Struct. Biol.* **131**, 38–43.
5. Thomas, J. L., Howloka, D., Baird, B. & Webb, W. W. (1994). Large-scale co-aggregation of fluorescent lipid probes with cell surface proteins. *J. Cell Biol.* **126**, 795–802.
6. Zurzolo, C., van Meer, G. & Mayor, S. (2003). The order of rafts. Conference on microdomains, lipid rafts and caveolae. *EMBO Rep.* **4**, 1117–1121.
7. Pralle, A., Keller, P., Florin, E.-L., Simons, K. & Hörber, J. K. H. (2000). Sphingolipid-cholesterol rafts diffuse as small entities in the plasma membrane of mammalian cells. *J. Cell Biol.* **148**, 997–1007.
8. Dietrich, C., Bagatolli, L. A., Volovyk, Z. N., Thompson, N. L., Levi, M., Jacobson, K. & Gratton, E. (2001). Lipid rafts reconstituted in model membranes. *Biophys. J.* **80**, 1417–1428.
9. Dietrich, C., Volovyk, Z. N., Levi, M., Thompson, N. L. & Jacobson, K. (2001). Partitioning of Thy-1, GM1 and crossed-linked phospholipid analogs into lipid rafts reconstituted in supported model membrane monolayers. *Proc. Natl Acad. Sci. USA*, **98**, 10642–10647.
10. Ribi, H. O., Ludwig, D. S., Mercer, K. L., Schoolnik, G. K. & Kornberg, R. D. (1988). Three-dimensional structure of cholera toxin penetrating a lipid membrane. *Science*, **239**, 1272–1276.
11. Anderson, R. G. W. & Jacobson, K. (2002). A role for lipid shells in targeting proteins to caveolae, rafts and other lipid domains. *Science*, **296**, 1821–1825.
12. Simons, K. & Vaz, W. L. C. (2004). Model systems, lipid rafts and cell membranes. *Annu. Rev. Biophys. Biomol. Struct.* **33**, 269–295.
13. Heerklotz, H., Szadkowska, H., Anderson, T. & Seelig, J. (2003). The sensitivity of lipid domains to small perturbations demonstrated by the effect of Triton. *J. Mol. Biol.* **329**, 793–799.
14. de Almeida, R. F. M., Fedorov, A. & Prieto, M. (2003). Sphingomyelin/phosphatidylcholine/cholesterol phase diagram: boundaries and composition of lipid rafts. *Biophys. J.* **85**, 2406–2416.
15. Veatch, S. L. & Keller, S. L. (2003). Separation of liquid phases in giant vesicles of ternary mixtures of phospholipids and cholesterol. *Biophys. J.* **85**, 3074–3083.
16. Veatch, S. L. & Keller, S. L. (2003). A closer look at the canonical "raft mixture" in model membrane studies. *Biophys. J.* **84**, 725–726.
17. Sot, J., Collado, M. I., Arrondo, J. L. R., Alonso, A. & Goñi, F. M. (2002). Triton X-100 resistant bilayers: effect of lipid composition and relevance to the raft phenomenon. *Langmuir*, **18**, 2828–2835.
18. Stryer, L. (1978). Fluorescence energy transfer as a spectroscopic ruler. *Annu. Rev. Biochem.* **47**, 819–846.
19. Loura, L. M. S., de Almeida, R. F. M. & Prieto, M. (2001). Detection and characterization of membrane microheterogeneity by resonance energy transfer. *J. Fluorescence*, **11**, 197–209.
20. Feigenson, G. W. & Buboltz, T. (2001). Ternary phase diagram of dipalmitoyl-PC/dilauroyl-PC/cholesterol: nanoscopic domain formation driven by cholesterol. *Biophys. J.* **80**, 2775–2788.
21. Silvius, J. R. (2003). Fluorescence energy transfer reveals microdomain formation at physiological temperatures in lipid mixtures modeling the outer leaflet of the plasma membrane. *Biophys. J.* **85**, 1034–1045.
22. Loura, L. M. S., Fedorov, A. & Prieto, M. (2000). Membrane probe distribution heterogeneity: a resonance energy transfer study. *J. Phys. Chem. B*, **104**, 6920–6931.
23. Loura, L. M. S., Fedorov, A. & Prieto, M. (2001). Fluid–fluid membrane microheterogeneity: a fluorescence resonance energy transfer study. *Biophys. J.* **80**, 776–788.
24. de Almeida, R. F. M., Loura, L. M. S., Fedorov, A. & Prieto, M. (2002). Non-equilibrium phenomena in the phase separation of a two-component lipid bilayer. *Biophys. J.* **82**, 823–834.
25. Medhage, B., Mukhtar, E., Kalman, B., Johansson, L.B.-Å. & Molotkovsky, J. G. (1992). Electronic energy transfer in anisotropic systems. Part 5—Rhodamine-lipid derivatives in model membranes. *J. Chem. Soc. Faraday Trans.* **88**, 2845–2851.
26. Snyder, B. & Freire, E. (1982). Fluorescence energy transfer in two dimensions: a numeric solution for random distributions. *Biophys. J.* **40**, 137–148.
27. Van der Meer, B., Coker, G., III & Chen, S.-Y.S. (1994). *Resonance Energy Transfer: Theory and Data*, VCH Publishers, New York.
28. McMullen, T. P. W., Lewis, R. N. A. H. & McElhaney, R. N. (2004). Cholesterol–phospholipid interactions, the liquid-ordered phase and lipid rafts in model and biological membranes. *Curr. Opin. Colloid Interface Sci.* **8**, 459–468.
29. Silvius, J. R., del Giudice, D. & Lafleur, M. (1996). Cholesterol at different bilayer concentrations can promote or antagonize lateral segregation of phospholipids of differing acyl chain length. *Biochemistry*, **35**, 15198–15208.
30. Abreu, M. S. C., Moreno, M. J. & Vaz, W. L. C. (2004). Kinetics and thermodynamics of association of a phospholipid derivative with lipid bilayers in liquid-disordered and liquid-ordered phases. *Biophys. J.* **87**, 353–365.
31. Vaz, W. L. C. & Melo, E. (2001). Fluorescence spectroscopic studies on phase heterogeneity in lipid bilayer membranes. *J. Fluorescence*, **11**, 255–271.
32. Yuan, C., Furlong, J., Burgos, P. & Johnston, L. J. (2002). The size of lipid rafts: an atomic force microscopy study of ganglioside GM1 domains in sphingomyelin/DOPC/cholesterol membranes. *Biophys. J.* **82**, 2526–2535.
33. Yuan, C. & Johnston, L. J. (2001). Atomic force microscopy studies of ganglioside GM1 domains in phosphatidylcholine and phosphatidylcholine/cholesterol bilayers. *Biophys. J.* **81**, 1059–1069.
34. Friedrichson, T. & Kurzchalia, T. V. (1998). Microdomains of GPI-anchored proteins in living cells revealed by crosslinking. *Nature*, **394**, 802–805.
35. Varma, R. & Mayor, S. (1998). GPI-anchored proteins are organized in submicron domains at the cell surface. *Nature*, **394**, 798–801.
36. Prior, I. A., Muncke, C., Parton, R. G. & Hancock, J. F. (2003). Direct visualization of Ras proteins in spatially distinct cell surface microdomains. *J. Cell Biol.* **160**, 165–170.
37. Heerklotz, H. (2002). Triton promotes domain formation in lipid raft mixtures. *Biophys. J.* **83**, 2693–2701.
38. London, E. (2001). Insights into lipid raft structure and formation from experiments in model membranes. *Curr. Opin. Struct. Biol.* **12**, 480–486.
39. Fujiwara, T., Ritchie, K., Murakoshi, H., Jacobson, K. & Kusumi, A. (2002). ??? *J. Cell Biol.* **157**, 1071–1081.
40. van Meer, G. (1998). Lipids of the Golgi membrane. *Trends Cell Biol.* **8**, 29–33.
41. Contreras, L. M., de Almeida, R. F. M., Fedorov, A.,

Villalaín, J. & Prieto, M. (2001). Interaction of α-melanocyte stimulating hormone with binary phospholipid membranes: structural changes and relevance of phase behavior. *Biophys. J.* **80**, 2273–2283.
42. Sklar, L. A., Hudson, B. S. & Simoni, R. D. (1977). Conjugated polyene fatty acids as fluorescent probes: synthetic phospholipid membrane studies. *Biochemistry*, **16**, 819–828.
43. Loura, L. M. S., de Almeida, R. F. M., Coutinho, A. & Prieto, M. (2003). Interaction of peptides with binary phospholipid membranes: application of fluorescence methodologies. *Chem. Phys. Lipids*, **122**, 77–96.
44. Wang, T.-Y. & Silvius, J. R. (2001). Cholesterol does not induce segregation of liquid-ordered domains in bilayers modeling the inner leaflet of the plasma membrane. *Biophys. J.* **84**, 367–378.
45. Ahmed, S. N., Brown, D. A. & London, E. (1997). On the origin of sphingolipid/cholesterol-rich detergent-insoluble cell membranes: physiological concentrations of cholesterol and sphingolipid induce formation of a detergent-insoluble, liquid-ordered lipid phase in model membranes. *Biochemistry*, **36**, 10944–10953.
46. McClare, C. W. F. (1971). An accurate and convenient organic phosphorus assay. *Anal. Biochem.* **39**, 527–530.
47. Sklar, L. A., Hudson, B. S., Petersen, M. & Diamond, J. (1977). Conjugated polyene fatty acids on fluorescent probes: spectroscopic characterization. *Biochemistry*, **16**, 813–818.
48. Lentz, B. R. (1988). Membrane "fluidity" from fluorescence anisotropy measurements. In *Spectroscopic Membrane Probes* (Loew, L. M., ed.), vol. 1, pp. 13–41, CRC, Boca Raton, FL.
49. Haugland, R. P. (1996). *Handbook of Fluorescent Probes, Research Chemicals* (6th edit.), Molecular Probes, Inc., Eugene, OR.
50. Gandhavadi, M., Allende, D., Vidal, A., Simon, S. A. & McIntosh, T. J. (2002). Structure, composition, and peptide binding properties of detergent soluble bilayers and detergent resistant rafts. *Biophys. J.* **82**, 1469–1482.
51. Chiu, S.-W., Jakobson, E., Subramaniam, S. & Scott, H. L. (1999). Combined Monte Carlo and molecular dynamics simulation of fully hydrated dioleoyl and palmitoyl-oleoyl phosphatidylcholine lipid bilayers. *Biophys. J.* **77**, 2462–2469.
52. Li, X.-M., Smaby, J. M., Momsen, M. M., Brockman, H. L. & Brown, R. E. (2000). Sphingomyelin interfacial behavior: the impact of changing acyl chain composition. *Biophys. J.* **78**, 1921–1931.
53. Smaby, J. M., Momsen, M. M., Brockman, H. L. & Brown, R. E. (1997). Phosphatidylcholine acyl unsaturation modulates the decrease in interfacial elasticity induced by cholesterol. *Biophys. J.* **73**, 1492–1505.

Edited by G. von Heijne

(Received 25 November 2004; received in revised form 13 December 2004; accepted 14 December 2004)